

Article

# Comparison between Virgin and Recycled 316L SS and AlSi10Mg Powders Used for Laser Powder Bed Fusion Additive Manufacturing

Shahir Mohd Yusuf , Edmund Choo and Nong Gao \*

Materials Research Group, Faculty of Engineering and Physical Sciences, University of Southampton, Southampton SO17 1BJ, UK; symy1g12@soton.ac.uk (S.M.Y.); eztc1a15@soton.ac.uk (E.C.)

\* Correspondence: N.Gao@soton.ac.uk; Tel.: +44-023-8059-3396

Received: 18 November 2020; Accepted: 1 December 2020; Published: 3 December 2020



**Abstract:** In this study, the comparison of properties between fresh (virgin) and used (recycled) 316L stainless steel (316L SS) and AlSi10Mg powders for the laser powder bed fusion additive manufacturing (L-PBF AM) process has been investigated in detail. Scanning electron microscopy (SEM), electron-dispersive X-ray spectroscopy (EDX), and X-ray diffraction (XRD) techniques are used to determine and evaluate the evolution of morphology, particle size distribution (PSD), circularity, chemical composition, and phase (crystal structure) in the virgin and recycled powders of both materials. The results indicate that both recycled powders increase the average particle sizes and shift the PSD to higher values, compared with their virgin powders. The recycled 316L SS powder particles largely retain their spherical and near-spherical morphologies, whereas more irregularly shaped morphologies are observed for the recycled AlSi10Mg counterpart. The average circularity of recycled 316L SS powder only reduces by ~2%, but decreases ~17% for the recycled AlSi10Mg powder. EDX analysis confirms that both recycled powders retain their alloy-specific chemical compositions, but with increased oxygen content. XRD spectra peak analysis suggests that there are no phase change and no presence of any undesired precipitates in both recycled powders. Based on qualitative comparative analysis between the current results and from various available literature, the reuse of both recycled powders is acceptable up to 30 times, but re-evaluation through physical and chemical characterizations of the powders is advised, if they are to be subjected for further reuse.

**Keywords:** virgin; recycled; metal powders; laser powder bed fusion; additive manufacturing

## 1. Introduction

Laser powder bed fusion (L-PBF) is one of the main categories of metal additive manufacturing (AM) technology, in which selective laser melting (SLM) is a widely used technique under this category. In the SLM process, a focused laser beam is used to selectively melt multiple layers of powder bed in succession and produce complex, functional metallic components according to the initial computer-aided-design (CAD) file [1]. To date, a wide range of metals and alloys have been successfully fabricated by SLM, including 316L SS, 304L SS, 15-5 PH SS, AlSi10Mg, Scalmalloy (AlMgSc), CoCr, IN 718, Ti6Al4V, and CuSn10 for various functional use, especially in the aerospace, biomedical, and automotive industries.

To date, a significant amount of research on metal AM has focused on the process–microstructure–property relationship. In particular, emphasis is given on the influence of various processing parameters such as laser power, scan speed, scan line (hatch) spacing, and layer thickness on the microstructures and the resulting properties such as fracture, yield, and tensile strengths, fatigue life, as well as corrosion and tribological properties [2–8]. Studies have shown that AM-fabricated metallic components

can possess similar or even enhanced properties, compared to conventionally manufactured (CM) parts [9–12]. Such improvements in these properties, e.g., strength, have been generally attributed to the unique multi-scale microstructures, much finer grain sizes, and the presence of ultrafine/nano-sized precipitates [13–20]. Furthermore, efforts for the standardization and qualification of metal AM parts have been actively carried out by organizations such as the American Society for Testing and Materials (ASTM) and the National Institute of Standards and Technology (NIST) by publishing various standards pertaining to additively manufactured metallic components [21–27].

While research into the process–microstructure–property relationship of AM metallic parts is certainly important, another equally essential aspect that has been given less attention is the properties of the metal powder used for AM processing, i.e., the feedstock materials. So far, available studies in the literature have revealed that the quality of these feedstock materials play a major role in determining the quality of the as-built AM parts, particularly densification levels and porosity contents [28–30]. In fact, the quality of metal powders used for AM is often assessed through their physical properties such as particle size, particle size distribution (PSD), morphology, packing density and flowability, as well as their chemical composition. In turn, the quality of metal powders is significantly determined by the powder manufacturing method, in which water atomization (WA), gas atomization (GA), and the plasma rotating electrode process (PREP) are prevalent techniques [28,31–35]. Nevertheless, for L-PBF AM, high packing density and high flowability are desired to ensure optimal powder melting and homogeneous deposition of the powder bed layers [36]. Thus, in terms of morphology, smooth, spherical particles with as little satellites/defects as possible are desirable [29,37–39]. In addition, Hajnys et al. [37], Liu et al. [40], and Benson et al. [41] explained that a wide PSD with a mix of large and fine particle sizes can improve the packing density of the powder bed through the accumulation of the fine powders within the interstitial spaces that exist around the larger powder particles. However, some studies have also shown slightly reduced flowability when a wide PSD is used for AM fabrication due to increased inter-particle friction, thereby suggesting that some compromise is needed when selecting the particle sizes to attain the highest possible packing density while maximizing flowability [42–44]. On the other hand, several researchers recommend different nominal powder particle sizes to be used as the starting feedstock for L-PBF AM processes, e.g., 10–60 [28], 10–45 [29], and 5–80  $\mu\text{m}$  [45]. Nonetheless, regardless of the particle size range chosen for AM processing, the powder particles need to be spherical and free from defects as mentioned previously.

On the other hand, back in 2016, Honeywell projected that the metal AM industry will experience an immense growth amounting to \$3.1 billion over the next 5–10 years [46]. However, the relatively high cost of virgin powders for L-PBF AM (~\$100–\$200/kg) and high usage volume per build (~40–50 kg is needed to fill the powder dispenser of the L-PBF machine) could be a major obstacle that could increase the overall production cost along the supply chain [47–52]. Thus, it is often economically viable to reuse/recycle the powders for further build cycles. However, the recycling of used powders may induce alterations in their physical properties and chemistry, which could affect the eventual mechanical properties of the as-built parts [27]. In fact, studies have shown that the recycled powders will almost always have larger particle sizes, rougher surface areas, reduced particle circularity, increased contamination, and a higher uptake of oxygen, nitrogen, or other inert gases regardless of the number of reuse times [53–61].

For example, Zhang et al. [47] attributed the rougher texture with the increased number of satellites in recycled 15-5 PH SS powder used for L-PBF to the repeated heating/cooling cycles during processing and increased inter-particle friction during powder bed recoating, as compared to its virgin counterpart. Galicki et al. [56] and Heiden et al. [57] both reported increased uptakes of oxygen in recycled 316L SS powder due to the oxidation that occurs during the manufacturing and the presence of residual oxygen in the build chamber. Similarly, Gorji et al. [38] detected an increase in the metal oxide content in recycled 316L SS powder, while the initially spherical particles evolved into a more irregularly shaped morphology, together with the presence of agglomerates and spatter. However, Mellin et al. [62] and Lutter-Gunther et al. [63] discovered an insignificant change in oxidation level in

recycled 316L SS powders, and hypothesized that the elements that have high affinity to oxygen such as Cr, Mn, and Fe diffuse out of the powder surface during the AM fabrication process. Nevertheless, any increased oxygen absorption and oxide formation need to be taken into consideration before reusing the recycled powders as they may adversely affect the performance of the eventual as-built parts during service [28,29]. On the other hand, Hajnys et al. [37] observed an increase in the PSD of recycled 316L SS powder but considered further reuse to be acceptable. Similarly, although Nezhadfar et al. [64] observed more of satellites and porosity on the surface of recycled 316L SS powder after 12 times of reuse, they reported an inconclusive trend in the ductility and mechanical strength in the solidified parts. Interestingly, some studies have also shown that a phase change could occur in recycled 316L SS and other SS alloys after >10 times of reuse without any considerable changes in the physical and chemical properties, as well as apparent density and hardness, implying that the recycled powders can still be reused for further build cycles [57,65].

Moreover, other direct investigations on the packing density and flowability of virgin and recycled powders for L-PBF based on established ASTM standards have shown some interesting results. For example, Seyda et al. [66] observed an increased flowability of recycled Ti6Al4V powder after 12 reuse times, which was attributed to the reduced number of satellites and fine particles despite the coarsening of the powder particles, which become increasingly irregularly shaped with increasing PSD values [66]. Quintana et al. [55] reported similar results in recycled Ti6Al4V powder with increasing content of oxygen from 0.09 wt.% to 0.13 wt.% after 31 reuse times. They even reported comparatively higher tensile strength in the parts built using the recycled powder due to the oxide strengthening effect. However, Tang et al. [67] revealed that while the Ti6Al4V powder particles became rougher and less spherical with fewer satellites after 21 build cycles, the PSD actually became narrower but still exhibited improved flowability without any compromise on the tensile properties in the as-built parts. In addition, Cordova et al. [36] studied the physical and chemical properties, as well as packing density and flowability, of virgin and recycled Ti6Al4V, AlSi10Mg, Scalmalloy, and IN 718 for various reuse times. In general, the recycled powders displayed an increased flowability and maintained a high packing density due to the reduced number of satellites and fine particles. They concluded that these would enable optimal powder melting and subsequently homogeneous deposition of the powders on the build platform.

Hence, these studies have shown the importance of evaluating and understanding the changes that occur in powders after undergoing numerous build cycles in terms of quality control and consideration for further reuse of the recycled powders for AM fabrication. However, comprehensive studies are still limited in terms of the correlation of the changes in the physical and chemical properties of virgin and recycled metal powders for AM processing, and their feasibility for further reuse [24,36,55]. Therefore, in this study, the physical and chemical properties of virgin and recycled 316L SS and AlSi10Mg powders used particularly for SLM processing were characterized and compared via the following approaches: (i) Microstructural observations through scanning electron microscopy (SEM), (ii) chemical composition analysis through electron-dispersive X-ray spectroscopy (EDX), and (iii) phase analysis through X-ray diffraction (XRD). The results from this study were then compared with those in the available literature to qualitatively assess the suitability of these recycled powders for further reuse.

## 2. Materials and Methods

Four batches of gas-atomized 316L SS and AlSi10Mg powders (2 fresh sets (virgin), and 2 used sets (recycled)) were used in this study. The fresh powders were obtained in their as-received state from the supplier, Concept Laser, while the recycled powders were taken from the powder dispenser container in the Laser Cusing M2 SLM machine. The following are the chemical compositions of the virgin powders as listed by Concept Laser (in wt.%): (i) 316L SS; Cr: 16.5–18.5; Ni: 10.0–13.0; Mo: 2.0–2.5; Mn: 0–2.0; Si: 0–1.0; P: 0–0.045; C: 0–0.03; S: 0–0.03; Fe: *Bal.* and (ii) AlSi10Mg; Si: 10.5–13.5; Mg: 0–0.05; Fe: 0–0.55; Mn: 0–0.35; Ti: 0–0.15; Cu: 0–0.05; Zn: 0–0.10; C: 0–0.05; Ni: 0–0.05; Pb: 0–0.05; Sn: 0–0.05, Al: *Bal.*

The recycled powders have been used about 20 times prior to collection. It should be noted that during the SLM process, the build chamber was purged with nitrogen to limit contamination and oxidation as much as possible. In addition, the recycled powders were also sieved for particles larger than 80  $\mu\text{m}$  for 316L SS, and 50  $\mu\text{m}$  for AlSi10Mg prior to characterization.

The size, morphology, circularity, and distribution of the virgin and recycled powder particles were evaluated via JSM-JEOL 9500 scanning electron microscopy (SEM, JEOL Tokyo, Japan) observations combined with analysis of the SEM images using ImageJ software (V 1.52, NIH and LOCI, Wisconsin, WI, USA). The changes in chemical composition between the virgin and recycled powders were assessed using EDX analysis, while phase evolution was determined through X-ray diffraction (XRD) analysis using a Bruker D2 Phaser powder diffraction machine ( $\theta/2\theta$  configuration, range: 40–100°, Bruker, Billerica, MI, USA).

### 3. Results and Discussion

#### 3.1. Microstructural Analysis

##### 3.1.1. Morphology and Distribution

The morphology and cumulative particle size distribution (PSD) of the virgin and recycled 316L SS and AlSi10Mg powders are shown in Figure 1. It is clear that the powder particles for both virgin powders are largely spherical or near-spherical (Figure 1a,d), but some irregularly shaped particles, such as cylindrical and tear-drop morphologies, can be observed for the virgin AlSi10Mg powders (Figure 1d). The surfaces of the recycled powders also appear rougher compared to the initially smooth virgin powders. In addition, fine particles called satellites (<5  $\mu\text{m}$ ) are attached to the surface of the virgin 316L SS and AlSi10Mg powders (e.g., dashed arrows of the zoomed areas in Figure 1a,d), which is common in virgin metallic powders produced by the gas atomization process [37,42,68]. However, fewer satellites are observed in both recycled powders as shown in Figure 1b,d, often attributed to their detachment from the surface of unmelted powder particles when they are being blown off from the as-built AM parts [27,55,67].

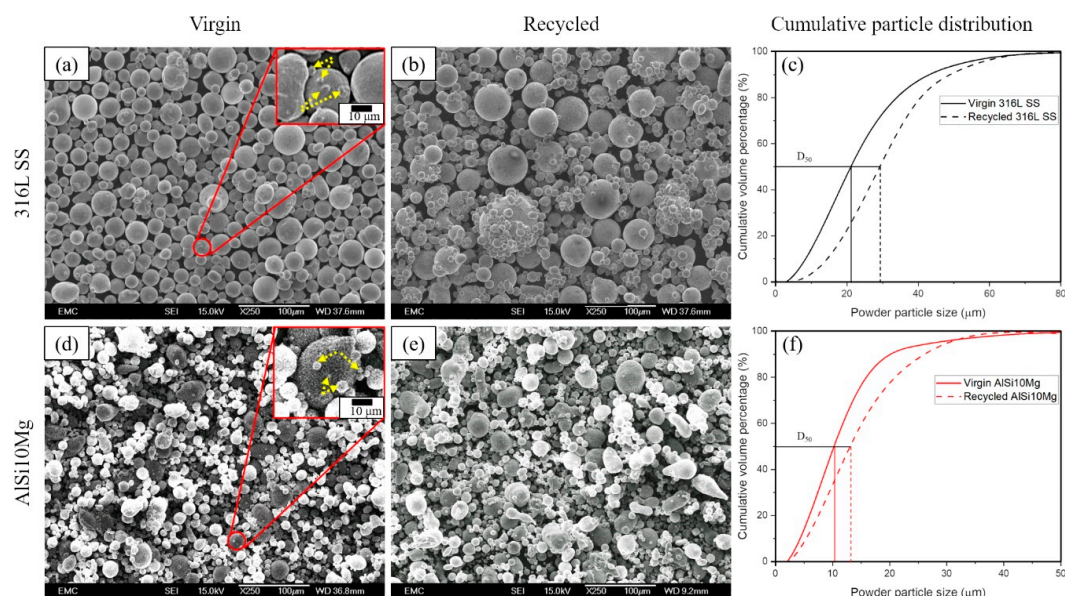


**Figure 1.** (a) Virgin, (b) recycled, and (c) cumulative particle size distribution of 316L SS powders; (d) virgin, (e) recycled, and (f) cumulative particle size distribution of AlSi10Mg powders. Dashed arrows of the zoomed areas inset of (a,d) show satellites on the surface of the virgin powders.

In addition, the agglomeration of small powder particles on the larger ones could be observed for the recycled 316L SS, as shown in Figure 1b. Such agglomerates are typically caused by the spattering of unmelted powders (powder spatter) from the powder bed upon contact with the laser heat source during SLM fabrication, which are then attached to other unconsolidated or semi-consolidated powder particles [36–38,47]. Similarly, other studies have shown that such agglomerates could also arise from melted powder particles that are ejected from the powder bed (droplet spatter), which eventually solidify during the flight and then either adhere to the as-fabricated part or impinge on other powder particles [69–72].

Although the recycled 316L SS powders largely retain their spherical/near-spherical shape (Figure 1b), the recycled AlSi10Mg powders generally deform into more irregular shapes (Figure 1e). Interestingly, the powder particles are apparently larger for both sets of recycled powders (Figure 1b,e) compared to their virgin counterparts (Figure 1a,d). This is also quantified by the cumulative distribution function showing the average particle size ( $D_{50}$ ) of the virgin and recycled powders (Figure 1c,f). The values of  $D_{50}$  for virgin and recycled 316L SS powders are  $\sim 22 \mu\text{m}$  and  $\sim 29 \mu\text{m}$ , respectively, which are higher than those of the virgin and recycled AlSi10Mg powders:  $\sim 11 \mu\text{m}$  and  $\sim 13 \mu\text{m}$ , respectively. These could be ascribed to the melting of smaller powder particles during the previous SLM processing [47]. The higher  $D_{50}$  values for the recycled powders in this study are similar to those obtained for various recycled AM metal powders observed in other studies, which often show a wider distribution and variation in particle sizes [36,58,59]. Nevertheless, Figure 2 indicates that the 316L SS powder consists of a wide range of particle sizes with broad size distribution (0–80  $\mu\text{m}$ ) when compared with the AlSi10Mg powder that comprises relatively finer particle sizes with narrower size distribution (0–50  $\mu\text{m}$ ).

On the other hand, several noteworthy observations can be made from the morphologies of the recycled 316L SS and AlSi10Mg powders shown by the high-magnification SEM images in Figure 2. For example, Figure 2a,d show the deformation of powders into more irregular shapes and visibly rougher surface texture compared to the initially smooth virgin powder particles. A number of factors have been related to these occurrences, including: (i) Continuous melting and cooling cycles of AM processing, (ii) remelting of powders upon exposure to the laser heat source, (iii) friction among powder particles during the spreading of successive powder bed layers, and long exposure times to high temperatures during the fabrication process [29,36,67,73].

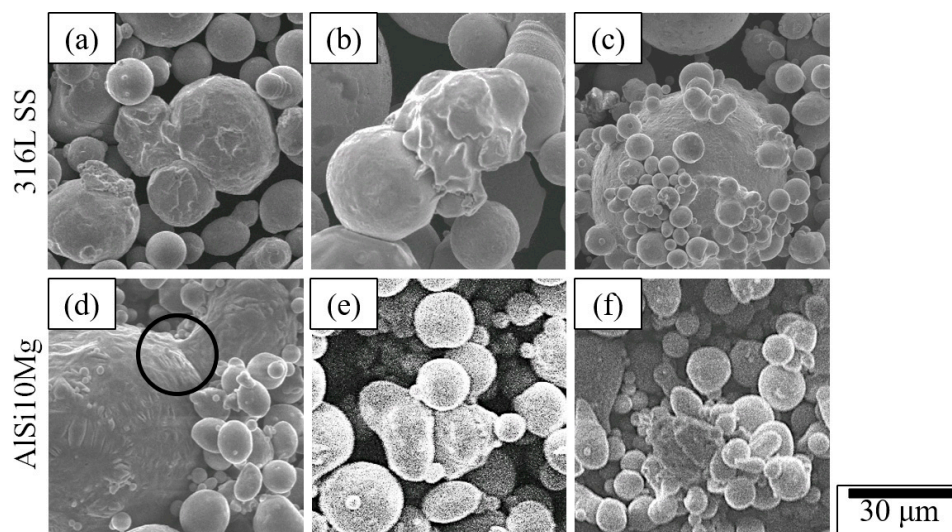


**Figure 2.** Examples of powder morphologies for recycled 316L SS (a–c) and AlSi10Mg (d–f): (a,d) Deformed powders, rough surface, and sintering necks (circled area in Figure 2d); (b,e) incomplete powder melting and fusion; and (c,f) powder agglomeration due to spatter.

In addition, a sintering neck can be observed to form between two adjacent powder particles of the recycled AlSi10Mg powders, as shown by the circled area in Figure 2d. Similarly, Figure 2b exhibits the fusion of a partially melted powder particle with an unmelted one for the recycled 316L SS, while an example of the incomplete fusion of differently sized powders in recycled AlSi10Mg is shown in Figure 2e. Altogether, the occurrence of these phenomena can be attributed to the insufficient heat input and considerable temperature difference between loose powders and powders that are already fused [74–76]. They have been identified as undesirable defects that contribute not only to the surface roughness of as-built AM parts, but also, more importantly, to the porosity that could compromise their strength and service properties [6,67,68,77].

Furthermore, the agglomeration of powder particles due to droplet and powder spatter, previously observed in Figure 1b,e, are shown in more detail in Figure 2c,f for recycled 316L SS and AlSi10Mg powders, respectively. In both cases, the size of the agglomerates is measured as  $>45\ \mu\text{m}$ . For 316L SS, much smaller powder particles ranging from 5 to 15  $\mu\text{m}$  are impinged on larger powder particles of  $>45\ \mu\text{m}$ . As for AlSi10Mg, particles with sizes of 5–20  $\mu\text{m}$  are observed to be clustered together, whereas larger particles remain either free from such agglomerates, or only have fewer satellites attached onto them. Interestingly, the clumped particles are of different morphologies that include spherical, near-spherical, and irregularly shaped ones. This is in contrast with the agglomerates in recycled 316L SS, in which much smaller spherical or near-spherical powder particles are attached to the larger powder particles with similar morphologies. These can be ascribed to the higher tendency of fine particle sizes with narrow size distribution to agglomerate, compared to those possessing comparatively larger particle sizes and wider size distribution, as is the case for the AlSi10Mg and 316L SS powders in this study, respectively [78,79].

Moreover, the histograms in Figure 3 reveal the PSD of the virgin and recycled 316L SS and AlSi10Mg powders in more detail. Both virgin and recycled 316L SS powders (Figure 3a,b) exhibit a comparatively wider size distribution than those of AlSi10Mg powders (Figure 3c,d), ranging from 0 to 80  $\mu\text{m}$  and 0 to 50  $\mu\text{m}$ , respectively. A clear shift toward higher PSD values, i.e., increasing percentages of larger particle sizes, can be observed:  $>25\ \mu\text{m}$  for 316L SS (Figure 3b) and  $>10\ \mu\text{m}$  for AlSi10Mg (Figure 3d). At the same time, fewer fine particles ranging from 0 to 5  $\mu\text{m}$  can be observed in the recycled powders (Figure 3b,d). This confirms the higher  $D_{50}$  values observed for the recycled powders shown by the cumulative PSD graphs Figure 1c,f, which can be attributed to the presence of agglomerates and the removal of satellites during AM fabrication [36,67].

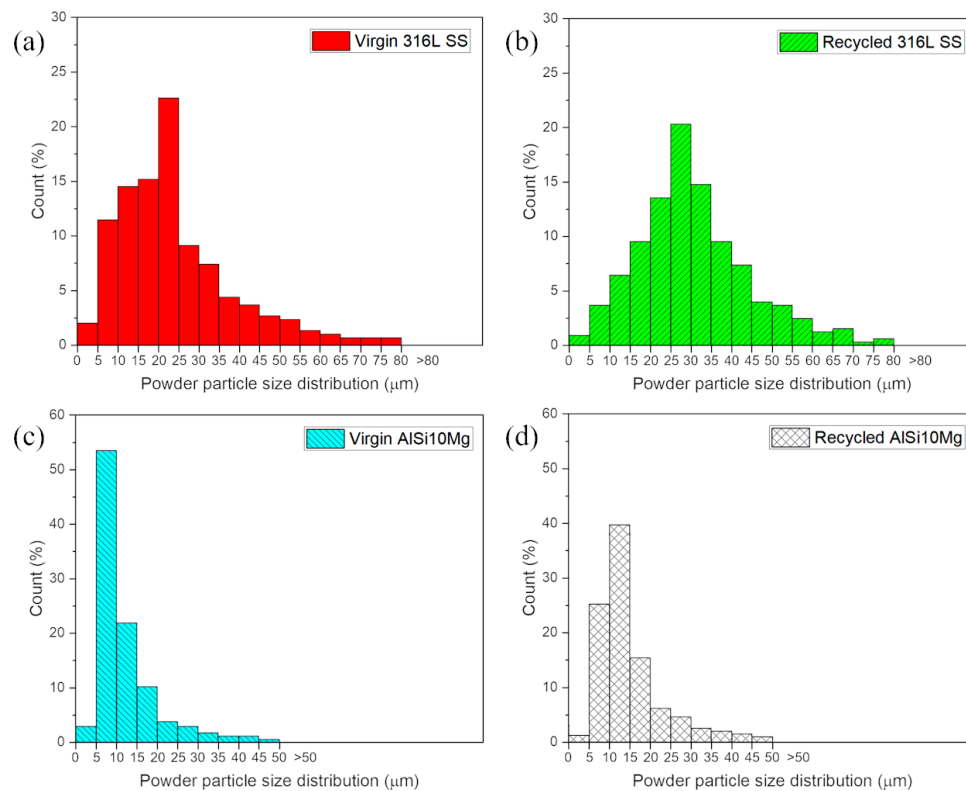


**Figure 3.** Powder particle size distribution of virgin and recycled 316L SS (a,b respectively) and AlSi10Mg (c,d respectively) powders.

### 3.1.2. Circularity

In addition to SEM observations that provide visual and qualitative assessments of the powder particle shapes, the circularity factor,  $C$ , is introduced to evaluate the morphology of the virgin and recycled 316L SS and AlSi10Mg powders, given by the formula [80]:

$$C = 4\pi A/P^2 \quad (1)$$

where  $P$  is the perimeter ( $\mu\text{m}$ ) and  $A$  is the pore area ( $\mu\text{m}^2$ ), both determined from the ImageJ software.  $C$  values close to 1 indicate near-perfect circular particles, while  $C$  values close to 0 demonstrate increasingly irregularly shaped particles. The results of the calculations are shown in Table 1.

**Table 1.** Average circularity of virgin and recycled 316L SS and AlSi10Mg powders.

Powder	Circularity		Percentage Reduction (%)
	Virgin	Recycled	
316L SS	$0.89 \pm 0.11$	$0.87 \pm 0.13$	2.3
AlSi10Mg	$0.83 \pm 0.17$	$0.69 \pm 0.31$	16.9

It is clear that the virgin powders possess higher average circularity values than the recycled powders, with a slightly higher value in 316L SS ( $0.89 \pm 0.11$ ) than AlSi10Mg ( $0.83 \pm 0.17$ ). This suggests rounder and more regular shapes in the virgin 316L SS compared to the virgin AlSi10Mg, confirming the SEM observations in Figure 1a,d. The average circularity of recycled 316L SS powder remains virtually unchanged at  $0.87 \pm 0.13$ , while that of recycled AlSi10Mg powder decreases to  $0.69 \pm 0.31$ . This correlates well with the observations in Figure 1b,d, in which the 316L SS powder particles largely retain their spherical or near-spherical shapes, whereas the AlSi10Mg powder particles tend to

deform into more irregular shapes upon reuse for SLM fabrication. On the other hand, representative visual examples of powder particle circularity are shown in Figure 4. A range of morphologies can be observed with the corresponding circularity, with the highest circularity,  $C = 1$ , obtained from virgin 316L SS powder (Figure 4a), and the lowest circularity was evaluated as  $C = 0.38$  from recycled AlSi10Mg powder (Figure 4e).

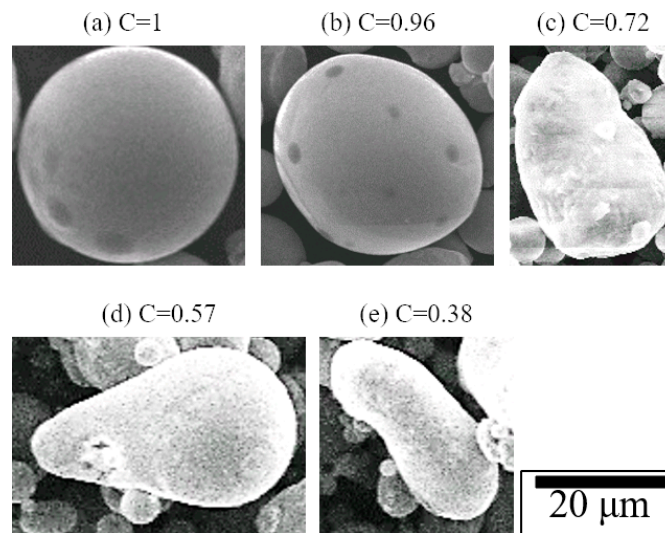


**Figure 4.** Examples of particle circularity for the metal powders used in this study. Representative images of (a,b) are taken from 316L SS, while those of (c–e) are taken from AlSi10Mg.

### 3.2. Compositional Analysis

Semi-quantitative EDX analysis was conducted on the surface of the virgin and recycled 316L SS and AlSi10Mg powders to determine their chemical compositions, and the results are presented in Table 2.

**Table 2.** Chemical composition of virgin and recycled powders via electron-dispersive X-ray spectroscopy (EDX) analysis (wt.%).

Element	316L SS		AlSi10Mg	
	Virgin	Recycled	Virgin	Recycled
Fe	61.71 ± 0.08	60.38 ± 0.05	-	-
Ni	12.92 ± 0.04	11.89 ± 0.05	-	-
Cr	18.43 ± 0.06	17.55 ± 0.03	-	-
Al	-	-	86.97 ± 0.07	86.16 ± 0.05
Si	0.94 ± 0.01	1.11 ± 0.02	11.09 ± 0.04	10.43 ± 0.03
Mg	-	-	0.45 ± 0.03	0.40 ± 0.04
Mn	1.96 ± 0.03	2.18 ± 0.01	-	-
Mo	2.46 ± 0.02	2.21 ± 0.03	-	-
O	1.42 ± 0.07	4.68 ± 0.09	1.49 ± 0.08	3.01 ± 0.08

It can be observed that the composition of the main elements in both virgin powders determined via EDX analysis (Table 2) corresponds well and is within the range of the supplier-listed compositions detailed in Section 2. In addition, the composition of most elements for the virgin and recycled powders only fluctuates slightly and remains stable, except for oxygen. For 316L SS, the oxygen content in the recycled powder increases by ~3 times compared to the virgin powder, whereas it doubles that of the virgin powder for the recycled AlSi10Mg. The increase in oxygen content in the recycled powders is expected and has been observed in various metal powders that have undergone AM processing in other studies [36,47,55,67]. The higher percentage of oxygen in recycled AM powders can be attributed

to a number of factors, including: (i) Oxygen pick-up due to contaminants, moisture, and residual oxygen that might still be present within the build chamber despite being purged with protective inert gases such as argon and nitrogen (this study); (ii) vaporization of oxygen (a trace element) from the powder surface that might already exist during powder production upon contact with the laser heat source; and (iii) the exposure of powder to ambient air during their removal from the as-received part, during the sieving process, as well as during powder handling and storage [36,38,67].

In particular, several studies in the field of powder metallurgy have also shown the strong affinity of major alloying elements such as Mn and Si to oxygen and the selective oxidization on the powder surface [81–83], which might also be the case for the 316L SS and AlSi10Mg powders subjected to AM fabrication in this study, respectively. In fact, Simonelli et al. [69] found that the high affinity of Mn and Si to oxygen was the reason that both elements were selectively oxidized on the surface of molten material spatter-ejected from the powder bed, which then solidify during flight in the build chamber. Nevertheless, further study could include EDX map analysis for visual confirmation of the presence of these oxides on the surface of these powders. In addition, an important thing to note is that EDX is commonly used as a semi-quantitative tool to determine the chemical composition of a material, but the exact values detected might not be accurate, particularly for trace elements such as oxygen [42,47,61]. Thus, more detailed surface chemical analysis is necessary, such as by using X-ray photoemission spectroscopy (XPS) and inductively coupled plasma mass spectrometry (ICP-MS), to obtain a more accurate reading of the chemical compositions, as well as to detect thin surface oxide layers that may be present on the surface of the powders [47,70]. Nonetheless, the EDX analysis in this study adequately captures the trend of increasing oxygen content in the recycled powders, and suggests that the deviations in chemical compositions are within the acceptable range for both materials [84,85].

### 3.3. Phase Analysis

The phase identification of the virgin and recycled 316L SS and AlSi10Mg powders is shown by the XRD spectra in Figure 5.

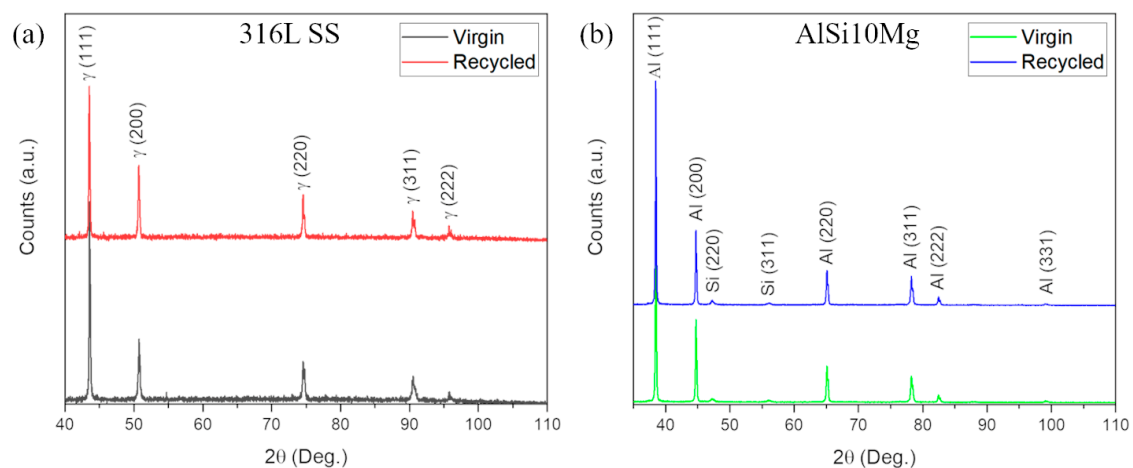


**Figure 5.** XRD spectra of virgin and recycled 316L SS (a) and AlSi10Mg (b) powders.

Figure 5a shows no phase change for both virgin and recycled 316L SS powder, such that they remain a single  $\gamma$ -austenite FCC structure. Similarly, the recycled AlSi10Mg powder exhibits identical peaks of Al and Si as the virgin counterpart (Figure 5b). No additional peaks can be observed, suggesting that any change in phase (if any) is below the XRD detection limit and represents very little contamination within the build chamber, and therefore, it is negligible [38,70]. However, the hypothesis of insignificant contamination during the AM build cycle might seem paradoxical, seeing that the EDX results show increasing oxygen content in the recycled powder that is often associated with the presence of contaminants inside the build chamber. Thus, the more reasonable explanation is that

even though no phase change can be observed in the XRD spectra, it could still occur but below the limit of detection of the XRD equipment used in this study. Furthermore, nitrogen is known as an austenite stabilizer and, especially for 316L SS, the presence of nitrogen in the build chamber during AM processing might even suppress the formation of other phases despite the three-fold increase in oxygen content detected by EDX analysis in the recycled powder.

In fact, Heiden et al. [57] conducted electron-backscattered diffraction (EBSD) and XRD analyses on virgin and recycled 316L SS and observed the presence of the  $\delta$ -ferrite BCC phase in the recycled powder (reused for 30 times). Jacob et al. [65] observed a progressive increase in ferritic-martensitic BCC phase in 17-4 PH stainless-steel powder via XRD analysis after a minimum use of four times. In addition, Simonelli et al. [69] detected an enrichment of thin Mn and Mg oxide films on the surface of recycled 316L SS and AlSi10Mg powders through EDX maps analysis, respectively. They attributed the growth of these oxide films to the volatile nature of Mn and Mg and their high affinity toward oxygen [5,60,86]. Therefore, future investigations could include carrying out EDX mapping, electron-backscattered diffraction (EBSD), and transmission electron microscopy (TEM) analyses to determine sub-micron-scale phase and microstructures, which can definitively confirm whether other phases can be observed in the recycled powders.

#### 4. Discussion

It is known that flowability and packing density are two of the most important qualities of metal powders that are to be used for PBF AM processing as they have considerable influence on the quality of as-built parts, together with the processing parameters applied [42,87,88]. Altogether, these two properties are determined by the particle size, PSD, morphology, and chemical composition of the powders [61,66,70]. However, with increasing number of uses, the virgin powders with initially favorable properties will undergo physical and chemical changes that require further evaluation before a decision can be made about whether they can be reused. Based on the guidelines proposed by Cordova et al. [36], it is recommended to consider the following five key aspects in assessing the suitability of reusing the powders, including: (i) Particle size distribution (PSD), (ii) powder morphology, (iii) chemical composition, (iv) flowability, and (v) packing density.

First, the nominal powder PSD typically used for SLM is in the range of 10–45  $\mu\text{m}$ , which is much finer than those used for other PBF processes, such as electron beam melting (EBM) (45–106  $\mu\text{m}$ ) and directed energy deposition (DED) (20–200  $\mu\text{m}$ ) [28,29,89]. This is because of the architecture of SLM machines that only allows for fine powder distributions to reduce surface roughness by utilizing lower layer thicknesses, as compared with those of EBM and DED counterparts that enable the use of higher layer thicknesses and larger particle sizes [90]. Based on the results in this study, the PSD for both recycled powders fall within this range, up to 80  $\mu\text{m}$  for 316L SS and up to 50  $\mu\text{m}$  for AlSi10Mg. In particular, the recycled 316L SS powder can be further sieved to remove the agglomerates and unmelted particle sizes of >45  $\mu\text{m}$ .

Secondly, powder morphology has been identified as another important aspect that needs to be examined as it significantly influences flowability and packing density. Smooth, spherical, and dry particles possess the best flowability characteristics due to the low inter-particle friction that enable the deposition of densely solidified layers and produces homogeneous microstructures [42,91]. On the other hand, powder particles with rough surfaces and more irregular shapes reveal larger specific surfaces that increase surface friction between them, typically reducing flowability and leaving voids and gaps that lead to porosity in the as-built parts [47,68]. Therefore, to be considered for further reuse, the guidelines provided by Cordova et al. [36] recommended that the circularity factor of the recycled powders needs to be as close to 1 as possible, or at least  $\geq 7.0$ . In this study, there are no issues with the recycled 316L SS powders as the average circularity is  $\sim 0.87$ , which does not differ much from its virgin counterpart ( $\sim 0.89$ ). However, the average circularity of recycled AlSi10Mg is  $\sim 0.69$ , which is on the borderline value suggested. Thus, the recycled AlSi10Mg might still be considered for a few more uses, but only for noncritical components outside of high-risk industries, e.g., in the aerospace

sector and some biomedical applications [38]. Furthermore, reuse after >30 build cycles is generally not recommended, due to severe degradation that deteriorates the quality of the metal powders, as has often been observed in powders of various metallic materials, including considerable agglomerates and satellites, and noticeable deformation and distortion into highly irregular shapes [55,57,68,92].

Thirdly, the chemical composition of the recycled powders must be measured to ensure that they remain within alloy-specific compositions, and to address the issues of losses due to evaporation such as spatter, contamination within the build chamber and during powder handling and recovery, as well as any pick-up of oxygen or other trace elements such as nitrogen or argon during the AM build process [29,36]. In addition, no (significant) phase change should occur in the recycled powder, as any changes in the crystal structure, e.g., through additional peaks in the XRD spectra, or any precipitates and oxide layers detected from TEM or XPS, would result in considerable contamination that could negatively impact the structural and mechanical properties of the fabricated parts [38,70]. In the present investigation, EDX analysis shows a 2–3 times increase in oxygen content for both recycled powders, which could be caused by residual oxygen present in the chamber, or evaporation of entrapped oxygen within the powders (from the gas atomization powder production process) due to powder and droplet spatter [1,93]. Nevertheless, the XRD spectra analysis does not show any unexpected peaks in the recycled powders, and their chemical compositions remain within the acceptable range of both 316L SS and AlSi10Mg alloys. Therefore, based on the EDX and XRD results, at least, the further reuse of both recycled powders is considered acceptable. However, if more detailed analyses such as through XPS, EBSD, EDX mapping, and TEM reveal undesired precipitates, oxides, or phases in the recycled powders, then the recycled powders should not be used for any structural or other critical end-use applications.

The last two guidelines from Cordova et al. [36] recommend the flowability and packing density of the recycled powders to be directly measured through analytical tools following the various ASTM or other international standards. High flowability and high packing density are desired to ensure homogeneous deposition of powder bed layers and optimal powder melting, which would lead to high densification and low porosity levels in the as-built parts. In particular, the packing density of the powder bed has been found to be more important than processing parameters such as laser power ( $P$ ), scan speed ( $S$ ), hatch spacing ( $d$ ), and layer thickness ( $h$ ) in determining part density and porosity [36,42]. Smooth and spherical particles with minimal defects are known to improve packing density, while irregularly shaped particles with numerous defects such as agglomerates and satellites reduce the packing density of the powder bed, similar to their influences on powder flowability [29,39,94]. In addition, the inclusion of fine powder particles (fines) also contributes to high packing density due to the fine particles filling the interstitial spaces that exist among the larger particles [40,44,90]. However, these fine particles tend to result in wider PSD and have been found to reduce powder flowability [30,36,55,67]. Therefore, as a compromise, it is suggested that smooth, spherical particles with as minimum defects as possible with narrower PSD should be used for AM fabrication to attain optimized flowability with relatively high packing density [29,37,42].

In this study, direct measurements of flowability and packing density were not carried out. However, comparative analysis between the current results and discussions with the first three recommendations from Cordova et al. [36], as well as with established literature, can still be made to provide qualitative assessments for the viability of reusing the recycled powders in this study (after 20 times of use). The properties of the recycled powders analyzed in this study, powder characteristics that are suitable for reuse as suggested by available literature, and recommendations from the authors regarding the possible further reuse of the recycled powders are listed in Table 3. Based on the comparative analysis, the authors suggest that the reuse of the recycled 316L SS and AlSi10Mg powders is acceptable up until 30 build cycles overall, but further reuse beyond that should require re-evaluation through further detailed physical and chemical characterizations.

**Table 3.** Qualitative analysis on the recommendation of reuse of the recycled powders in the present study based on results established in available literature.

Powder Properties	Recommendation from Literature	Properties of Recycled Powders in This Study		Overall Recommendation from Current Authors
		316L SS	AlSi10Mg	
PSD	10–45 $\mu\text{m}$ ; Narrow PSD; reduced fine particles [29,36,37,42]	0–80 $\mu\text{m}$ (Wide PSD); reduced fine particles of sizes < 5 $\mu\text{m}$	0–50 $\mu\text{m}$ (Narrower PSD); reduced fine particles sizes <5 $\mu\text{m}$	PSD for both powders are acceptable. Particles >45 $\mu\text{m}$ can be further sieved, as they are mostly agglomerates anyway.
Morphology and circularity	Smooth, spherical, with minimum defects (agglomerates and satellites); circularity as close to 1 as possible or at least $\geq 0.7$ [36,37,42,92]	Mostly spherical and near-spherical; agglomerates present; fewer satellites; circularity: $\sim 0.87$ (virgin: $\sim 0.89$ )	Mix of spherical and increasingly irregular-shaped particles; agglomerates present; fewer satellites; circularity: $\sim 0.69$ (virgin: 0.83)	No issues for 316L SS powder. Exercise caution when reusing AlSi10Mg powder, probably not more than 30 times overall, and not for critical components.
Chemical composition and phase (crystal structure)	Maintain within alloy-specific compositions; minimum pick-up of oxygen or other trace elements; No change from initial powders and no undesired precipitates should form [29,36,38,70,91]	Within alloy-specific composition; oxygen content triples from that of initial powders; No phase change from initial powders can be detected through XRD	Within alloy-specific composition; oxygen content doubles from that of initial powders; No phase change from initial powders can be detected through XRD	Reuse of both recycled powders is acceptable based on the EDX and XRD results, but there are concerns on the oxygen pick-up. Detailed analysis through XPS, EDX mapping, EBSD, and TEM could be carried out in the future to definitively confirm the presence of any undesired phases/precipitates.

## 5. Conclusions

In this study, the properties of 316L SS and AlSi10Mg powders in the virgin condition and recycled state after 20 times of reuse are analyzed and compared by using SEM, EDX, and XRD techniques. Qualitative assessments on the viability of using the recycled powders for further build cycles are made based on the results in this study and those recommended in the available literature. The following conclusions can be made:

- (1) Compared with virgin powders, a shift to higher particle size distribution (PSD) values are observed, resulting in higher average particle sizes for both 316L SS and AlSi10Mg recycled powders.
- (2) SEM observations indicate the presence of agglomerates, but fewer satellites are detected on the surface of the recycled 316L SS and AlSi10Mg powders.
- (3) The recycled 316L SS powder particles retain their spherical and near-spherical morphologies, whereas that of the AlSi10Mg counterpart deforms into more irregularly shaped morphologies.
- (4) The average circularity of recycled 316L SS powder only reduces slightly by ~2%, but a higher reduction in circularity is attained for the recycled AlSi10Mg powder (~17%).
- (5) EDX analysis suggests the chemical composition of both recycled powders remains within alloy-specific values, but an increase in oxygen pick-up is detected in both cases.
- (6) XRD spectra peak analyses indicate no change in crystal structures or presence of any undesired precipitates in both recycled powders.
- (7) Based on the present results and qualitative comparative analysis with available literature, the reuse of both recycled powder for further build cycles is acceptable up to 30 overall build cycles. However, these are preliminary assessments, and extensive re-evaluation through physical and chemical characterizations is necessary if they are to be further reused.

**Author Contributions:** S.M.Y. contributes primarily to the writing and compilation of manuscript and data analysis; E.C. contributes primarily to carrying out the main experiments and data collection; N.G. is heavily involved in the project conceptualization, administration, and planning, as well as the review and editing of the manuscript. All authors have read and agreed to the published version of the manuscript.

**Funding:** This research received no external funding.

**Conflicts of Interest:** The authors declare no conflict of interest.

## References

1. Yusuf, S.M.; Gao, N. Influence of energy density on metallurgy and properties in metal additive manufacturing. *Mater. Sci. Technol.* **2017**, *33*, 1269–1289. [[CrossRef](#)]
2. Frazier, W.E. Metal additive manufacturing: A review. *J. Mater. Eng. Perform.* **2014**, *23*, 1917–1928. [[CrossRef](#)]
3. Herzog, D.; Seyda, V.; Wycisk, E.; Emmelmann, C. Additive manufacturing of metals. *Acta Mater.* **2016**, *117*, 371–392. [[CrossRef](#)]
4. Manakari, V.; Parande, G.; Gupta, M. Selective laser melting of magnesium and magnesium alloy powders: A review. *Metals* **2016**, *7*, 2. [[CrossRef](#)]
5. Olakanmi, E.O. Selective laser sintering/melting (SLS/SLM) of pure Al, Al–Mg, and Al–Si powders: Effect of processing conditions and powder properties. *J. Mater. Process. Technol.* **2013**, *213*, 1387–1405. [[CrossRef](#)]
6. Olakanmi, E.O.; Cochrane, R.F.; Dalgarno, K.W. A review on selective laser sintering/melting (SLS/SLM) of aluminium alloy powders: Processing, microstructure, and properties. *Prog. Mater. Sci.* **2015**, *74*, 401–477. [[CrossRef](#)]
7. Sun, Y.; Moroz, A.; Alrbaey, K. Sliding wear characteristics and corrosion behaviour of selective laser melted 316L stainless steel. *J. Mater. Eng. Perform.* **2013**, *23*, 518–526. [[CrossRef](#)]
8. Bartolomeu, F.; Buciumeanu, M.; Pinto, E.; Alves, N.; Carvalho, O.; Silva, F.; Miranda, G. 316L stainless steel mechanical and tribological behavior—A comparison between selective laser melting, hot pressing and conventional casting. *Addit. Manuf.* **2017**, *16*, 81–89. [[CrossRef](#)]
9. Lewandowski, J.J.; Seifi, M. Metal additive manufacturing: A review of mechanical properties. *Annu. Rev. Mater. Res.* **2016**, *46*, 151–186. [[CrossRef](#)]

10. Gorsse, S.; Hutchinson, C.; Gouné, M.; Banerjee, R. Additive manufacturing of metals: A brief review of the characteristic microstructures and properties of steels, Ti-6Al-4V and high-entropy alloys. *Sci. Technol. Adv. Mater.* **2017**, *18*, 584–610. [[CrossRef](#)] [[PubMed](#)]
11. Boisselier, D.; Sankaré, S. Influence of powder characteristics in laser direct metal deposition of SS316L for metallic parts manufacturing. *Phys. Procedia* **2012**, *39*, 455–463. [[CrossRef](#)]
12. Song, B.; Zhao, X.; Li, S.; Han, C.; Wei, Q.; Wen, S.; Liu, J.; Shi, Y. Differences in microstructure and properties between selective laser melting and traditional manufacturing for fabrication of metal parts: A review. *Front. Mech. Eng.* **2015**, *10*, 111–125. [[CrossRef](#)]
13. Saeidi, K.; Gao, X.; Zhong, Y.; Shen, Z. Hardened austenite steel with columnar sub-grain structure formed by laser melting. *Mater. Sci. Eng. A* **2015**, *625*, 221–229. [[CrossRef](#)]
14. Chen, N.; Ma, G.; Zhu, W.; Godfrey, A.; Shen, Z.; Wu, G.; Huang, X. Enhancement of an additive-manufactured austenitic stainless steel by post-manufacture heat-treatment. *Mater. Sci. Eng. A* **2019**, *759*, 65–69. [[CrossRef](#)]
15. Tucho, W.M.; Cuvillier, P.; Sjolyst-Kverneland, A.; Hansen, V. Microstructure and hardness studies of Inconel 718 manufactured by selective laser melting before and after solution heat treatment. *Mater. Sci. Eng. A* **2017**, *689*, 220–232. [[CrossRef](#)]
16. Tucho, W.M.; Lysne, V.H.; Austbø, H.; Sjolyst-Kverneland, A.; Hansen, V. Investigation of effects of process parameters on microstructure and hardness of SLM manufactured SS316L. *J. Alloys Compd.* **2018**, *740*, 910–925. [[CrossRef](#)]
17. Olakanmi, E.O.; Cochrane, R.F.; Dalgarno, K.W. Densification mechanism and microstructural evolution in selective laser sintering of Al-12Si powders. *J. Mater. Process. Technol.* **2011**, *211*, 113–121. [[CrossRef](#)]
18. Hadadzadeh, A.; Baxter, C.; Amirkhiz, B.S.; Mohammadi, M. Strengthening mechanisms in direct metal laser sintered AlSi10Mg: Comparison between virgin and recycled powders. *Addit. Manuf.* **2018**, *23*, 108–120. [[CrossRef](#)]
19. Hadadzadeh, A.; Amirkhiz, B.S.; Mohammadi, M. Contribution of Mg<sub>2</sub>Si precipitates to the strength of direct metal laser sintered AlSi10Mg. *Mater. Sci. Eng. A* **2019**, *739*, 295–300. [[CrossRef](#)]
20. Chen, B.; Moon, S.; Yao, X.; Bi, G.; Shen, J.; Umeda, J.; Kondoh, K. Strength and strain hardening of a selective laser melted AlSi10Mg alloy. *Scr. Mater.* **2017**, *141*, 45–49. [[CrossRef](#)]
21. Seifi, M.; Christiansen, D.; Beuth, J.; Harrysson, O.; Lewandowski, J.J. Process mapping, fracture and fatigue behaviour of Ti-6Al-4V produced by EBM additive manufacturing. In *Proceedings of the 13th World Conference on Titanium*; Venkatesh, V., Pilchak, A.L., Allison, J.E., Ankem, S., Boyer, R.R., Christodoulou, J., Fraser, H.L., Imam, M.A., Kosaka, Y., Rack, H.J., Eds.; The Minerals, Metals & Materials Society: Pittsburgh, PA, USA, 2016; pp. 1373–1378.
22. Seifi, M.; Salem, A.; Beuth, J.; Harrysson, O.; Lewandowski, J.J. Overview of materials qualification needs for metal additive manufacturing. *JOM J. Manag.* **2016**, *68*, 747–764. [[CrossRef](#)]
23. Seifi, M.; Gorelik, M.; Waller, J.; Hrabe, N.; Shamsaei, N.; Daniewicz, S.; Lewandowski, J.J. Progress towards metal additive manufacturing standardization to support qualification and certification. *JOM* **2017**, *69*, 439–455. [[CrossRef](#)]
24. Slotwinski, J.A.; Garboczi, E.; Hebenstreit, K.M. Porosity measurements and analysis for metal additive manufacturing process control. *J. Res. Natl. Inst. Stand. Technol.* **2014**, *119*, 494–528. [[CrossRef](#)] [[PubMed](#)]
25. Slotwinski, J.; Moylan, S. *Applicability of Existing Materials Testing Standards for Additive Manufacturing Materials*; NIST National Institute for Standards and Technology: Gaithersburg, MD, USA, 2014.
26. Hrabe, N.; Barbosa, N.; Daniewicz, S.; Shamsaei, N. *Findings from the NIST/ASTM Workshop on Mechanical Behavior of Additive Manufacturing Components*; NIST/ASTM: Gaithersburg, MD, USA, 2016. [[CrossRef](#)]
27. Brien, M.O. Existing standards as the framework to qualify additive manufacturing of metals. In *Proceedings of the IEEE Aerospace Conference, Big Sky, MT, USA, 3–10 March 2018*; pp. 1–10.
28. DebRoy, T.; Wei, H.L.; Zuback, J.S.; Mukherjee, T.; Elmer, J.W.; Milewski, J.O.; Beese, A.M.; Wilson-Heid, A.; De, A.; Zhang, W. Additive manufacturing of metallic components—Process, structure and properties. *Prog. Mater. Sci.* **2018**, *92*, 112–224. [[CrossRef](#)]
29. Sames, W.J.; List, F.A.; Pannala, S.; Dehoff, R.R.; Babu, S.S. The metallurgy and processing science of metal additive manufacturing. *Int. Mater. Rev.* **2016**, *61*, 315–360. [[CrossRef](#)]
30. Santecchia, E.; Spigarelli, S.; Cabibbo, M. Material reuse in laser powder bed fusion: Side effects of the laser—Metal powder interaction. *Metals* **2020**, *10*, 341. [[CrossRef](#)]

31. Sames, W.J.; Medina, F.; Peter, W.H.; Babu, S.S.; Dehoff, R.R. Effect of process control and powder quality on IN 718 produced using Electron Beam Melting. In *8th International Symposium on Superalloy 718 and Derivatives*; Wiley: Hoboken, NJ, USA, 2014; pp. 409–423. [[CrossRef](#)]
32. Zhao, X.; Chen, J.; Lin, X.; Huang, W. Study on microstructure and mechanical properties of laser rapid forming Inconel 718. *Mater. Sci. Eng. A* **2008**, *478*, 119–124. [[CrossRef](#)]
33. Qi, H.; Azer, M.; Ritter, A. Studies of standard heat treatment effects on microstructure and mechanical properties of laser net shape manufactured INCONEL 718. *Metall. Mater. Trans. A Phys. Metall. Mater. Sci.* **2009**, *40*, 2410–2422. [[CrossRef](#)]
34. Ahmed, F.; Ali, U.; Sarker, D.; Marzbanrad, E.; Choi, K.; Mahmoodkhani, Y.; Toyserkani, E. Study of powder recycling and its effect on printed parts during laser powder-bed fusion of 17-4 PH stainless steel. *J. Mater. Process. Technol.* **2020**, *278*, 116522. [[CrossRef](#)]
35. Morgan, C.; Stokes, R.; Priddy, M.; Khanzadeh, M.K.; Bian, L.; Mazur, J.Y.T., II; Yadollahi, A.; Doude, H.; Hammond, V.H. Influence of recycling and process parameters on powder characteristics of direct energy deposition Ti-6Al-4V. In *Proceedings of the Additive Manufacturing with Powder Metallurgy*, Phoenix, AZ, USA, 23–26 June 2019; p. 538.
36. Cordova, L.; Campos, M.; Tinga, T. Revealing the effects of powder reuse for selective laser melting by powder characterization. *JOM J. Manag.* **2019**, *71*, 1062–1072. [[CrossRef](#)]
37. Hajnys, J.; Pagac, M.; Mesicek, J.; Petru, J.; Spalek, F. Research of 316L metallic powder for use in SLM 3D printing. *Adv. Mater. Sci.* **2020**, *20*, 5–15. [[CrossRef](#)]
38. Gorji, N.E.; O'Connor, R.; Brabazon, D. XPS, XRD, and SEM characterization of the virgin and recycled metallic powders for 3D printing applications. In *Proceedings of the IOP Conference Series: Materials, Science and Engineering*, Iasi, Romania, 19–22 June 2019; p. 591. [[CrossRef](#)]
39. Romero, C.; Yang, F.; Bolzoni, L. Fatigue and fracture properties of Ti alloys from powder-based processes—A review. *Int. J. Fatigue* **2018**, *117*, 407–419. [[CrossRef](#)]
40. Liu, B.; Wildman, R.; Tuck, C.; Ashcroft, I.; Hague, R. Investigation the effect of particle size distribution on processing parameters optimisation in selective laser melting process. In *Proceedings of the 22nd Annual International Solid Freeform Fabrication Symposium—An Additive Manufacturing Conference SFF*, Austin, TX, USA, 8–10 August 2011; pp. 227–238.
41. Benson, J.M.; Snyders, E. The need for powder characterisation in the additive manufacturing industry and the establishment of a national facility. *South Afr. J. Ind. Eng.* **2015**, *26*, 104–114. [[CrossRef](#)]
42. Sutton, A.T.; Kriewall, C.S.; Leu, M.C.; Newkirk, J.W. Powders for additive manufacturing processes: Characterization techniques and effects on part properties. *Solid Free. Fabr.* **2016**, *1*, 1004–1030.
43. Sutton, A.T.; Kriewall, C.S.; Leu, M.C.; Newkirk, J.W. Powder characterisation techniques and effects of powder characteristics on part properties in powder-bed fusion processes. *Virtual Phys. Prototyp.* **2017**, *12*, 3–29. [[CrossRef](#)]
44. Simmons, J.C.; Chen, X.; Azizi, A.; Daeumer, M.A.; Zavalij, P.Y.; Zhou, G.; Schiffres, S.N. Influence of processing and microstructure on the local and bulk thermal conductivity of selective laser melted 316L stainless steel. *Addit. Manuf.* **2020**, *32*, 100996. [[CrossRef](#)]
45. Beese, A.M.; Carroll, B.E. Review of mechanical properties of Ti-6Al-4V made by laser-based additive manufacturing using powder feedstock. *JOM J. Manag.* **2015**, *68*, 724–734. [[CrossRef](#)]
46. Quigley, E.; Luo, Z.; Murella, A.; Lee, W.L.; Adams, J.; Tasooji, A. *Effect of Powder Reuse on DMLS (Direct Metal Laser Sintering) Product Integrity: Why Honeywell Believes the Future is Additive Manufacturing*; Arizona State University: Tempe, AZ, USA, 2016.
47. Zhang, J.; Hu, B.; Zhang, Y.; Guo, X.; Wu, L.; Park, H.-Y.; Lee, J.-H.; Jung, Y.-G. Comparison of virgin and reused 15-5 PH stainless steel powders for laser powder bed fusion process. *Prog. Addit. Manuf.* **2018**, *3*, 11–14. [[CrossRef](#)]
48. Liu, P.; Huang, S.H.; Mokasdar, A.; Zhou, H.; Hou, L. The impact of additive manufacturing in the aircraft spare parts supply chain: Supply chain operation reference (scor) model based analysis. *Prod. Plan. Control.* **2013**, *25*, 1169–1181. [[CrossRef](#)]
49. Durach, C.F.; Kurpjuweit, S.; Wagner, S.M. The impact of additive manufacturing on supply chains. *Int. J. Phys. Distrib. Logist. Manag.* **2017**, *47*, 954–971. [[CrossRef](#)]
50. Yusuf, S.M.; Cutler, S.; Gao, N. Review: The impact of metal additive manufacturing on the aerospace industry. *Metals* **2019**, *9*, 1286. [[CrossRef](#)]

51. Khajavi, S.H.; Partanen, J.; Holmström, J. Additive manufacturing in the spare parts supply chain. *Comput. Ind.* **2014**, *65*, 50–63. [[CrossRef](#)]
52. Ghadge, A.; Karantoni, G.; Chaudhuri, A.; Srinivasan, A. Impact of additive manufacturing on aircraft supply chain performance. *J. Manuf. Technol. Manag.* **2018**, *29*, 846–865. [[CrossRef](#)]
53. Costa-Silva, B.; Aiello, N.M.; Ocean, A.J.; Singh, S.; Zhang, H.; Thakur, B.K.; Becker, A.; Hoshino, A.; Mark, M.T.; Molina, H.; et al. Pancreatic cancer exosomes initiate pre-metastatic niche formation in the liver. *Nat. Cell Biol.* **2015**, *17*, 816–826. [[CrossRef](#)] [[PubMed](#)]
54. Shen, Y.F.; Jia, N.; Wang, Y.D.; Sun, X.; Zuo, L.; Raabe, D. Suppression of twinning and phase transformation in an ultrafine grained 2 GPa strong metastable austenitic steel: Experiment and simulation. *Acta Mater.* **2015**, *97*, 305–315. [[CrossRef](#)]
55. Quintana, O.A.; Alvarez, J.; McMillan, R.; Tong, W.; Tomonto, C. Effects of reusing Ti-6Al-4V powder in a selective laser melting additive system operated in an industrial setting. *JOM J. Manag.* **2018**, *70*, 1863–1869. [[CrossRef](#)]
56. Galicki, D.; List, F.; Babu, S.S.; Plotkowski, A.; Meyer, H.M.; Seals, R.; Hayes, C. Localized changes of stainless steel powder characteristics during selective laser melting additive manufacturing. *Metall. Mater. Trans. A Phys. Metall. Mater. Sci.* **2019**, *50*, 1582–1605. [[CrossRef](#)]
57. Heiden, M.J.; Deibler, L.A.; Rodelas, J.M.; Koepke, J.R.; Tung, D.J.; Saiz, D.J.; Jared, B.H. Evolution of 316L stainless steel feedstock due to laser powder bed fusion process. *Addit. Manuf.* **2019**, *25*, 84–103. [[CrossRef](#)]
58. Spierings, A.B.; Voegtlin, M.; Bauer, T.; Wegener, K. Powder flowability characterisation methodology for powder-bed-based metal additive manufacturing. *Prog. Addit. Manuf.* **2015**, *1*, 9–20. [[CrossRef](#)]
59. Hausnerova, B.; Mukund, B.N.; Sanetnik, D. Rheological properties of gas and water atomized 17-4PH stainless steel MIM feedstocks: Effect of powder shape and size. *Powder Technol.* **2017**, *312*, 152–158. [[CrossRef](#)]
60. Louvis, E.; Fox, P.; Sutcliffe, C.J. Selective laser melting of aluminium components. *J. Mater. Process. Technol.* **2011**, *211*, 275–284. [[CrossRef](#)]
61. Ardila, L.C.; Garcíandia, F.; González-Díaz, J.B.; Álvarez, P.; Echeverria, A.; Petite, M.M.; Deffley, R.; Ochoa, J. Effect of IN718 recycled powder reuse on properties of parts manufactured by means of Selective Laser Melting. *Phys. Procedia* **2014**, *56*, 99–107. [[CrossRef](#)]
62. Mellin, P.; Shvab, R.; Strondl, A.; Randelius, M.; Brodin, H.; Hryha, E.; Nyborg, L. COPGLOW and XPS investigation of recycled metal powder for selective laser melting. *Powder Metall.* **2017**, *60*, 223–231. [[CrossRef](#)]
63. Lutter-Günther, M.; Gebbe, C.; Kamps, T.; Seidel, C.; Reinhart, G. Powder recycling in laser beam melting: Strategies, consumption modeling and influence on resource efficiency. *Prod. Eng.* **2018**, *12*, 377–389. [[CrossRef](#)]
64. Nezhadfar, P.D.; Soltani-Tehrani, A.; Shamsaei, N. Effect of preheating build platform on microstructure and mechanical properties of additively manufactured 316L stainless steel. In Proceedings of the 30th Annual International Solid Freeform Fabrication Symposium—An Additive Manufacturing Conference, Austin, TX, USA, 12–14 August 2019; pp. 415–425.
65. Jacob, G.; Brown, C.; Donmez, A.; Watson, S. *Effects of Powder Recycling on Stainless Steel Powder and Built Material Properties in Metal Powder Bed Fusion Processes*; NIST Advanced Manufacturing Series 100-6; NIST National Institute of Standard and Technology: Gaithersburg, MD, USA, 2016; pp. 1–51.
66. Seyda, V.; Kaufmann, N.; Emmelmann, C. Investigation of aging processes of Ti-6Al-4V powder material in laser melting. *Phys. Procedia* **2012**, *39*, 425–431. [[CrossRef](#)]
67. Tang, H.P.; Qian, M.; Liu, N.; Zhang, X.Z.; Yang, G.Y.; Wang, J. Effect of powder reuse times on additive manufacturing of Ti-6Al-4V by selective electron beam melting. *JOM J. Manag.* **2015**, *67*, 555–563. [[CrossRef](#)]
68. Sun, Y.Y.; Gulizia, S.; Oh, C.H.; Doblin, C.; Yang, Y.F.; Qian, M. Manipulation and characterization of a novel titanium powder precursor for additive manufacturing applications. *JOM J. Manag.* **2015**, *67*, 564–572. [[CrossRef](#)]
69. Simonelli, M.; Tuck, C.; Aboulkhair, N.T.; Maskery, I.; Ashcroft, I.; Wildman, R.D.; Hague, R. A study on the laser spatter and the oxidation reactions during selective laser melting of 316L stainless steel, Al-Si10-Mg, and Ti-6Al-4V. *Metall. Mater. Trans. A Phys. Metall. Mater. Sci.* **2015**, *46*, 3842–3851. [[CrossRef](#)]
70. Terrassa, K.L.; Haley, J.C.; MacDonald, B.E.; Schoenung, J.M. Reuse of powder feedstock for directed energy deposition. *Powder Technol.* **2018**, *338*, 819–829. [[CrossRef](#)]

71. Jelis, E.; Clemente, M.; Kerwien, S.; Ravindra, N.M.; Hespos, M.R. Metallurgical and mechanical evaluation of 4340 steel produced by direct metal laser sintering. *JOM J. Manag.* **2015**, *67*, 582–589. [[CrossRef](#)]
72. Andani, M.T.; Dehghani, R.; Karamooz-Ravari, M.R.; Mirzaeifar, R.; Ni, J. A study on the effect of energy input on spatter particles creation during selective laser melting process. *Addit. Manuf.* **2018**, *20*, 33–43. [[CrossRef](#)]
73. Slotwinski, J.A.; Garboczi, E.J. Metrology needs for metal additive manufacturing powders. *JOM J. Manag.* **2015**, *67*, 538–543. [[CrossRef](#)]
74. Morrow, B.M.; Lienert, T.J.; Knapp, C.M.; Sutton, J.O.; Brand, M.J.; Pacheco, R.M.; Livescu, V.; Carpenter, J.S.; Gray, G.T., III. Impact of defects in powder feedstock materials on microstructure of 304L and 316L stainless steel produced by additive manufacturing. *Metall. Mater. Trans. A* **2018**, *49*, 3637–3650. [[CrossRef](#)]
75. Harun, W.S.W.; Manam, N.S.; Kamariah, M.S.I.N.; Sharif, S.; Zulkifly, A.H.; Ahmad, I.; Miura, H. A review of powdered additive manufacturing techniques for Ti-6al-4v biomedical applications. *Powder Technol.* **2018**, *331*, 74–97. [[CrossRef](#)]
76. Acharya, R.; Sharon, J.A.; Staroselsky, A. Prediction of microstructure in laser powder bed fusion process. *Acta Mater.* **2017**, *124*, 360–371. [[CrossRef](#)]
77. Mower, T.M.; Long, M.J. Mechanical behavior of additive manufactured, powder-bed laser-fused materials. *Mater. Sci. Eng. A* **2016**, *651*, 198–213. [[CrossRef](#)]
78. Simchi, A. The role of particle size on the laser sintering of iron powder. *Metall. Mater. Trans. B* **2004**, *35*, 937–948. [[CrossRef](#)]
79. Thejane, K.; Chikosha, S.; Du Preez, W.B. Characterisation and monitoring of Ti6AL4V (ELI) powder used in different selective laser melting systems. *S. Afr. J. Ind. Eng.* **2017**, *28*, 161–171. [[CrossRef](#)]
80. Lavery, N.P.; Cherry, J.; Mehmood, S.; Davies, H.; Girling, B.; Sackett, E.; Brown, S.G.R.; Sienz, J. Effects of hot isostatic pressing on the elastic modulus and tensile properties of 316L parts made by powder bed laser fusion. *Mater. Sci. Eng. A* **2017**, *693*, 186–213. [[CrossRef](#)]
81. Wilson, P.R.; Chen, Z. Characterisation of surface grain boundary precipitates formed during annealing of low carbon steel sheets. *Scr. Mater.* **2005**, *53*, 119–123. [[CrossRef](#)]
82. Wilson, P.R.; Chen, Z. The effect of manganese and chromium on surface oxidation products formed during batch annealing of low carbon steel strip. *Corros. Sci.* **2007**, *49*, 1305–1320. [[CrossRef](#)]
83. Hryha, E.; Gierl, C.; Nyborg, L.; Danninger, H.; Dudrova, E. Surface composition of the steel powders pre-alloyed with manganese. *Appl. Surf. Sci.* **2010**, *256*, 3946–3961. [[CrossRef](#)]
84. Brooks, J.A.; Thompson, A.W. Microstructural development and solidification cracking susceptibility of austenitic stainless steel welds. *Int. Mater. Rev.* **1991**, *36*, 16–44. [[CrossRef](#)]
85. Trevisan, F.; Calignano, F.; Lorusso, M.; Pakkanen, J.; Aversa, A.; Ambrosio, E.P.; Lombardi, M.; Fino, P.; Manfredi, D. On the selective laser melting (SLM) of the AlSi10Mg alloy: Process, microstructure, and mechanical properties. *Materials* **2017**, *10*, 76. [[CrossRef](#)]
86. Hryha, E.; Dudrova, E.; Nyborg, L. Critical aspects of alloying of sintered steels with manganese. *Metall. Mater. Trans. A Phys. Metall. Mater. Sci.* **2010**, *41*, 2880–2897. [[CrossRef](#)]
87. Bauereiß, A.; Scharowsky, T.; Körner, C. Defect generation and propagation mechanism during additive manufacturing by selective beam melting. *J. Mater. Process. Technol.* **2014**, *214*, 2522–2528. [[CrossRef](#)]
88. Pohlman, N.A.; Roberts, J.A.; Gonser, M.J. Characterization of titanium powder: Microscopic views and macroscopic flow. *Powder Technol.* **2012**, *228*, 141–148. [[CrossRef](#)]
89. Zekovic, S.; Dwivedi, R.; Kovacevic, R. Numerical simulation and experimental investigation of gas-powder flow from radially symmetrical nozzles in laser-based direct metal deposition. *Int. J. Mach. Tools Manuf.* **2007**, *47*, 112–123. [[CrossRef](#)]
90. Slotwinski, J.A.; Garboczi, E.; Stutzman, P.; Ferraris, C.F.; Watson, S.S.; Peltz, M.A. Characterization of metal powders used for additive manufacturing. *J. Res. Natl. Inst. Stand. Technol.* **2014**, *119*, 460–493. [[CrossRef](#)]
91. Strondl, A.; Lyckfeldt, O.; Brodin, H.; Ackelid, U. Characterization and control of powder properties for additive manufacturing. *JOM J. Manag.* **2015**, *67*, 549–554. [[CrossRef](#)]
92. Gaytan, S.M.; Murr, L.E.; Medina, F.; Martinez, E.; Lopez, M.I.; Wicker, R.B. Advanced metal powder based manufacturing of complex components by electron beam melting. *Mater. Technol.* **2009**, *24*, 180–190. [[CrossRef](#)]
93. Yusuf, S.M.; Chen, Y.; Boardman, R.; Yang, S.; Gao, N. Investigation on porosity and microhardness of 316L stainless steel fabricated by selective laser melting. *Metals* **2017**, *7*, 64. [[CrossRef](#)]

94. Cleary, P.W.; Sawley, M.L. DEM modelling of industrial granular flows: 3D case studies and the effect of particle shape on hopper discharge. *Appl. Math. Model.* **2002**, *26*, 89–111. [[CrossRef](#)]

**Publisher's Note:** MDPI stays neutral with regard to jurisdictional claims in published maps and institutional affiliations.



© 2020 by the authors. Licensee MDPI, Basel, Switzerland. This article is an open access article distributed under the terms and conditions of the Creative Commons Attribution (CC BY) license (<http://creativecommons.org/licenses/by/4.0/>).